Chapter 4: Pacific Concentric Global Ring Structures

Abstract
Nine prominent linear features imaged by satellite across the Pacific Ocean floor, identified as “Fracture Zones,” form parts of 19 concentric global ring structures with a common center in northern Siberia. Features from Landsat images are compared with bathymetry and gravity anomaly data, and together these suggest structures consistent with distant annulus resulting from the shock and release wave of a large impact. Such annulus will be referred to as Concentric Global Ring Structures.

Introduction

Cratering on earth is thought to be obscured by resurfacing of the continents and deep oceans. Google Earth provides high-resolution Landsat images of land and sonar imaging of submarine ocean surfaces from National Oceanic and Atmospheric Administration (NOAA). Additional resources from Scripps Institute of Oceanography (2014) and University of California San Diego include Global Gravity Anomaly (GGA) and Vertical Gravity Gradient maps displaying as overlays on Google Earth.

The GGA mapping is a valuable compliment to Landsat imaging, acquired using “slight variations of the pull of gravity… [as] recorded with satellite altimetry (Sandwell and Smith 2009).” Comparison of GGA with Vertical Gravity Gradient has shown GGA reflects lithologic differences, while Vertical Gravity Gradient recognized in wells where it produced “anomalous vertical gradient” reflecting “small extraneous effects of surface topography (Beyer 1971, page iii).” Minzhang et al. (2014) compared Vertical Gravity Gradient to high-intensity ship soundings for a small area in the northwest Pacific Ocean and found it to be highly consistent with topography. Vertical Gravity Gradient, reflecting higher resolution topography (Figure. 4.1A), shows a multitude of topographic linears on the ocean floor. Pairs of black arrows identify portions of fracture zones being considered. Figure 4.1B, shows in Vertical Gravity Gradient the location of plotted center for fracture zones as determined in Chapter 3. Landsat, and GGA maps, Figures 4.2 and 3, complement each other in evaluating evidence for lineaments.

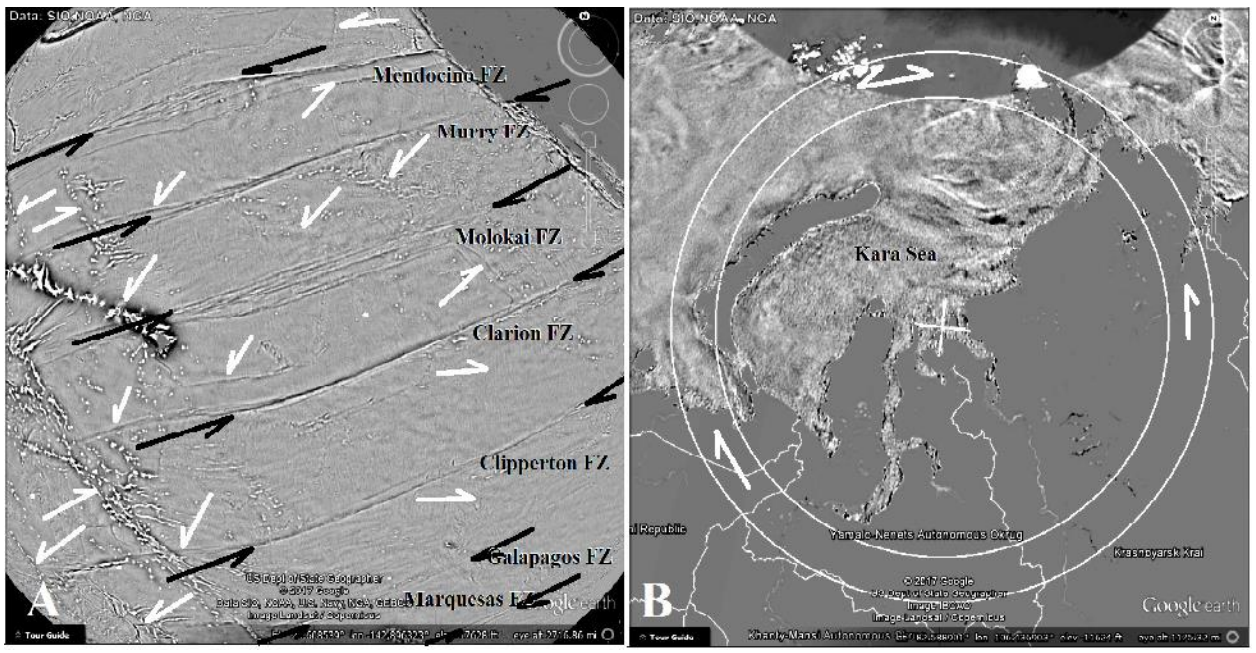

Figure 4.1: Vertical Gravity Gradient image showing (A) bathymetry of Pacific Ocean. This paper will discuss linears between black arrows. White arrows point to other bathymetric linears not included in this study and assumed to belong to other centers. (B) Bathymetry of Yenisei Bay, Kara Sea, Siberia, showing location of plotted center, Chapter 3, for Fracture Zones. Line of islands between pair of arrows on right and linear of ridge on left between concentric circles are first ring from center. (Image credit: Overlay for Google Earth, Scripps 2014, accessed 11/4/2017.)

As early as 1972 Meyerhoff and Meyerhoff (page 337) recognized that a “few areas of the ocean basins have linear magnetic anomalies” which are “approximately concentric” and “strike into the continents in at least 15 places.” And, Smoot (1999) characterized the sea floor as containing “linear chains” of what he called “megatrends.” Both were speaking of the Pacific Ocean as their figures show. I will extend these concentric linear structures through the continents and Atlantic Ocean, suggesting they are global. I propose Concentric Global Ring Structures (CGRS) as a name for groupings of concentric Small Circle megashears that circle the Earth and share a common center. As megashears, CGRS record the expenditure of shear energy. Barnhart (2017) theorized that these features were from impacts, recording in topographic energy variations consistent with the earth’s surface boundary interactions. If the energy source was great enough the expression would continue around the globe. Mapping these CGRS’s extent will determine if they are global.

The Pacific CGRS

Images from Google Earth

Figure 4.2 shows 19 lines (A & 1-18) that cross the Pacific Ocean basin, generally east-west. They also appear in GGA images (Figure 4.3), but some are more visible in the Vertical Gravity Gradient image (Figure 4.1A). They appear to be generally concentric and roughly equally spaced north to south. Labeled as fracture zones (FZ), segments of these lines have been studied for years, interpreted as Plate Tectonic features. This paper will refer to these lineaments as CGRS, associated by their concentric paths and shared center.

As shown in Chapter 3, using a program written by Maarten ‘t Hart (personal communications) for plotting circles of equal distance from a center on Google Earth, three points were chosen on the Murry (Figure 4.7) and Molokai FZ (Figure 4.11) using their south high-side linear. The Mendocino FZ (Figure 4.4) was avoided because I did not then know what to do with the abrupt southeast turn on its east end. The poles for the circles produced were close in the Kara Sea, Siberia and the area was searched for features that might relate to smaller circles (Figures 4.1B and 4.14). Coordinates for each of the FZ were taken and the resultant circles were searched for clues to their validity along much of their circumference. An abundance of concentric linears were located in many areas of rock exposure providing confidence (Chapter 2). Cultivated and vegetative land provided too much disruption for small linears. Many linears located were not concentric and were reasoned to belong to other centers.

Assuming the 8 FZ might be related and share poles, CGRS were plotted, and for the sections outside of the FZ the most probable location was estimated from GGA and Vertical Gravity Gradient maps and averaged spacing. Close-up topographic imaging (Figure 4.23) was used to identify the shock-release wave originated in the north.

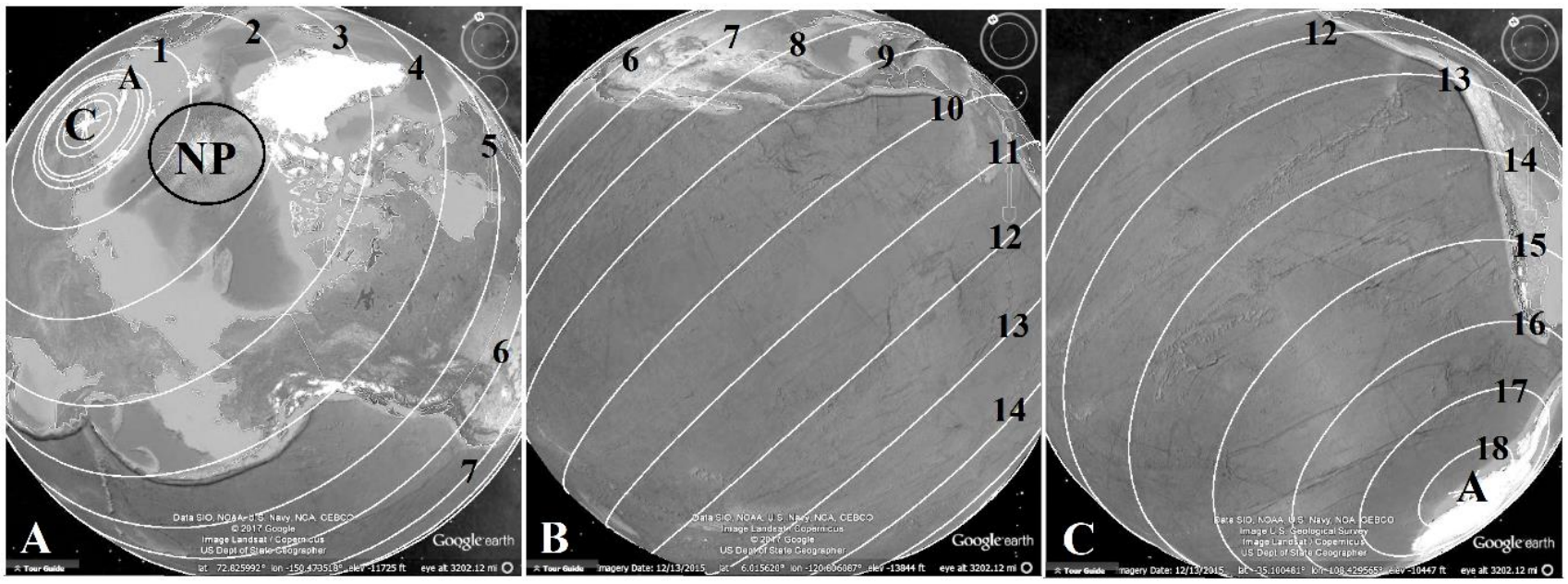

Figure 4.2: Google Earth images with overlay of Pacific CGRS showing numbering used in this paper. (A) North Pole (NP), with mapped center at Kara Sea, northern Siberia. Center (black C) is upper left. (B) Central Pacific with North America at top. (C) South Pacific with South America upper right, and antipode (black A) in lower right. White lines represent idealized paths of PGRS. (Image credit: Google Earth, accessed 11/1/2017.)

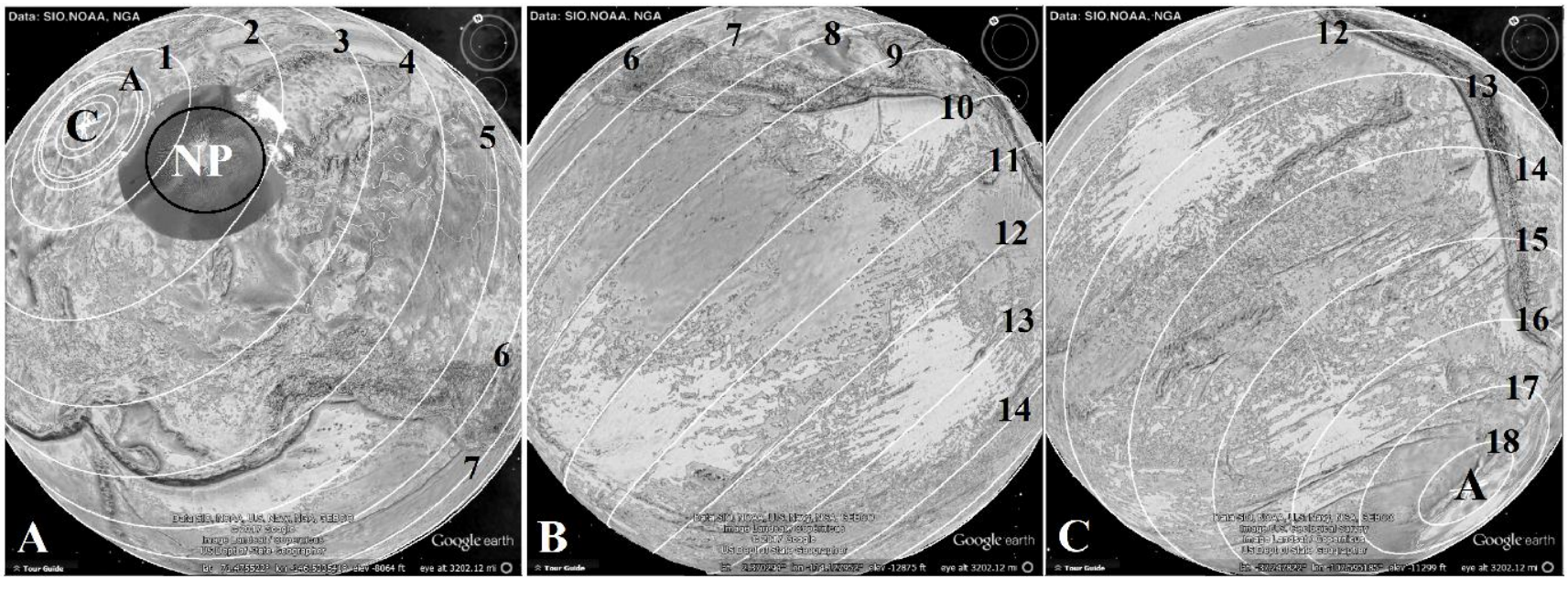

Figure 4.3: Pacific CGRS seen on GGA overlay, which highlights more detail of the ocean crust and emphasizes the multitude of linears visible on its depth. Images mirror those in Figure 4.2. (Image credit: Scripps 2014, Google Earth, accessed 11/1/2017.)

For simplicity, any CGRS with a number in this paper will refer to Pacific CGRS as represented by global positioning coordinate for the center and one point on each (Table I, Figures 4.2 and 4.3). A natural lineament will show some deviation in the distance from the center but not in its general concentric nature (Figures 4.6A and 4.10A).

	Latitude N	Longitude E	Distance from last ring	Fracture Zones
Center	72.7085°	78.0330°		
A	68.6219°	99.0017°	900 km 560 miles	
1	69.1690°	128.5178°	940 km 585 miles	
2	65.4350°	148.8365°	930 km 578 miles	
3	63.1265°	-178.0891°	1,150 km 715 miles	
4	56.9115°	-158.3566°	1,090 km 678 miles	
5	35.1545°	159.0067°	1,050 km 652 miles	Chinook
6	38.9217°	-157.4193°	900 km 560 miles	Mendocino
7	29.6688°	-152.5439°	1100 km 684 miles	Murry
8	22.7052°	-144.9364°	920 km 572 miles	Molokai
9	15.3950°	-142.0826°	860 km 534 miles	Clarion
10	4.3549°	-144.9628°	1120 km 696 miles	Clipperton
11	-3.7798°	-141.7004°	960 km 597 miles	Galapagos
12	-12.5270°	-142.6565°	930 km 578 miles	Marquesas
13	-23.7904°	-148.4457°	1050 km 652 miles	Austral
14	-32.6453°	-135.1997°	1,280 km 795 miles	
15	-44.5273°	-136.1716°	1,230 km 764 miles	
16	-53.2989°	-130.3152°	1,060 km 640 miles	
17	-61.4999°	-127.5337°	890 km 553 miles	
18	-65.9216°	-109.0359°	850 km 528 miles	

Table 4.1: Points on CGRS, which along with the center can be used to reproduce the small circles associated with the fracture zones indicated

While FZ are the most recognizable geomorphic features on each individual CGRS path, most wander from an exclusive association with the paths shown on Figures 4.2 and 4.3. Gay (2012) showed that fault expression may move from one linear to another at square intersection points, and I will propose the same for FZ. Altai Scarp, Chapter 3, ring to Mare Nectaris on the moon, illustrates limited movement of ring that should be expected where later impacts have cratered, Figure 3.12-3.15. Table 1 provides the named FZ that is associated with each continuous CGRS for reference purposes.

Tracing PGRS around the globe

FZ 6-13 exhibit generally similar wave lengths, ranging from 860 km (534 miles) to 1,280 km. (795 miles), a difference of 25%, with a mean of 980 km (608 miles). This paper will consider 980-1000 km to be the average wave length.

Pacific CGRS 6, Mendocino FZ

Figures 4 and 5 show details of CGRS 6. It is most obvious where it coincides with the Mendocino Fracture Zone. However, the Mendocino FZ turns to the southeast nearing the west coast of California (Figure 4.4). That turn reflects joining of another CGRS centered east of the Pacific center. The juxtaposition of several linears southeast of the x in Figure 4.4 suggest a plastic interaction of lineaments, which suggest additional discrete impacts occurred in a limited interval of time for those impacts to interact plastically through the energy envelope of their CGRS.

Figure 4.4: Google Earth image of CGRS 6 in the North Pacific where its path coincides with the Mendocino FZ. X = point on Table 1. (Image credit: Vertical Gravity Gradient, Scripps 2014, accessed 4/28/2016.)

Figure 4.5 shows CGRS 6 as it crosses the Mid-Atlantic Ridge (MAR). Note concentric linears to it (thin dashed lines) are interpreted as a wave train producing by interference from other CGRS. Chapter 2 noted that the repetition of concentric linears from a wave train confirms direction of a wave, even as they mask its singular expression.

The step pattern of the MAR is attributed to passing of the CGRS labelled here as “transform” faults by Atwater et al (1993) and another CGRS approximately perpendicular together forming the MAR. That a Pacific CGRS coincide with these faults in the Atlantic Ocean is a major coincidence or argues for a common origin.

Figure 4.5: Google Earth image showing CGRS 6 where it crosses the Mid-Atlantic Ridge. Solid black stepped line is MAR as normally portrayed; dark dotted line shows lineament. Thin dashed line to west indicate additional linear concentric to MAR. “Transform” linear in lower left is not concentric to CGRS 6. (Google Earth, accessed 4/28/2016.)

Figure 4.6 compares the distribution of smaller linears associated with CGRS 6 as plotted in the Pacific Ocean, through two separate areas of the North American, to the MAR in the Atlantic. While linears are not continuously visible across the North American continent, they are consistent enough, even in these smaller lineaments, to feel confident in identifying CGRS 6 as global.

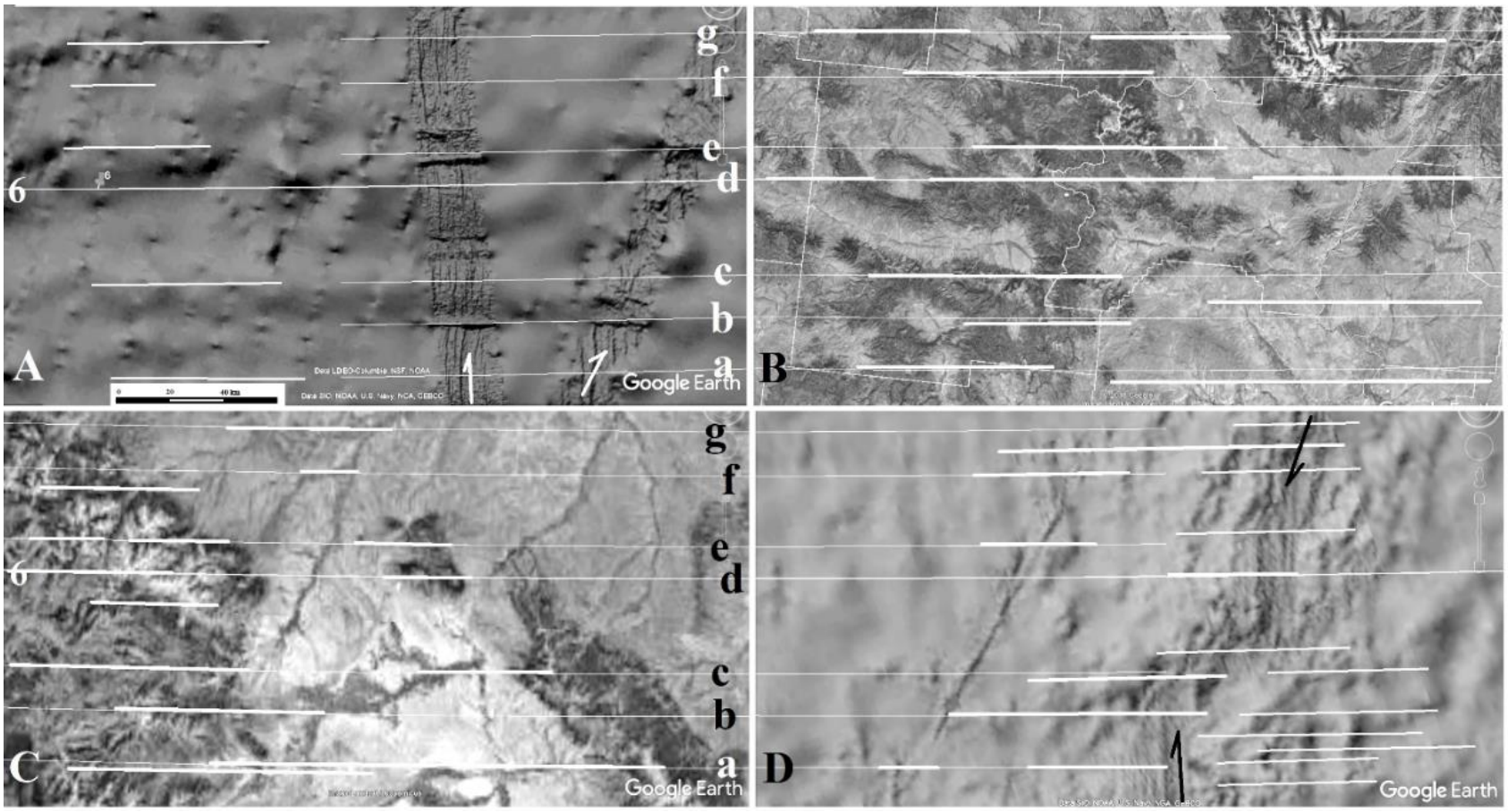

Figure 4.6: Four views of CGRS 6 and associated linears. Bolder white lines indicate regions of linear expression. (A) Mendocino FZ showing the natural deviation, mid Pacific. White arrows indicate zones of greater detail from NOAA, not geomorphic structure. (B) Mountains of Eastern Oregon. (C) Mountains of Montana-Wyoming's border. (D) Mid Atlantic Ridge region. Black arrows indicate MAR. (Image credit: Google Earth 2018, A: 38.909689°N, -156.418943°E, B: 44.430159°N, -119.084746°E, C: 44.773551°N, -109.390693°E, D: 35.830172°N, -34.564489°E. December 13, 2015, accessed 3/28/2018.)

Pacific CGRS 7 Murry FZ

Figure 4.7 shows CGRS 7 along the Murry FZ. The fracture zones are ridges and troughs up to 120 km wide (75 miles) in this area, and interpreted as remnants of the movement of the Pacific Plate (Atwater 1970, Atwater et al 1993, Austermann et al 2011). I propose the ridge and trough are expressions of the shock and release wave being broken up to a short wave train. The divergence of the FZ to the west and many less-pronounced linears testify of much interference.

Figure 4.7: Google Earth image of CGRS 7 mid Pacific Ocean along the Murry FZ. X = coordinate from Table I. (Google Earth, accessed 4/28/2016.)

Figure 4.8 shows CGRS 7 where it crosses the Mid-Atlantic Ridge. Although its path is not as obvious as the expression of CGRS 6 to the north, numerous concentric linears do attest to its expression here.

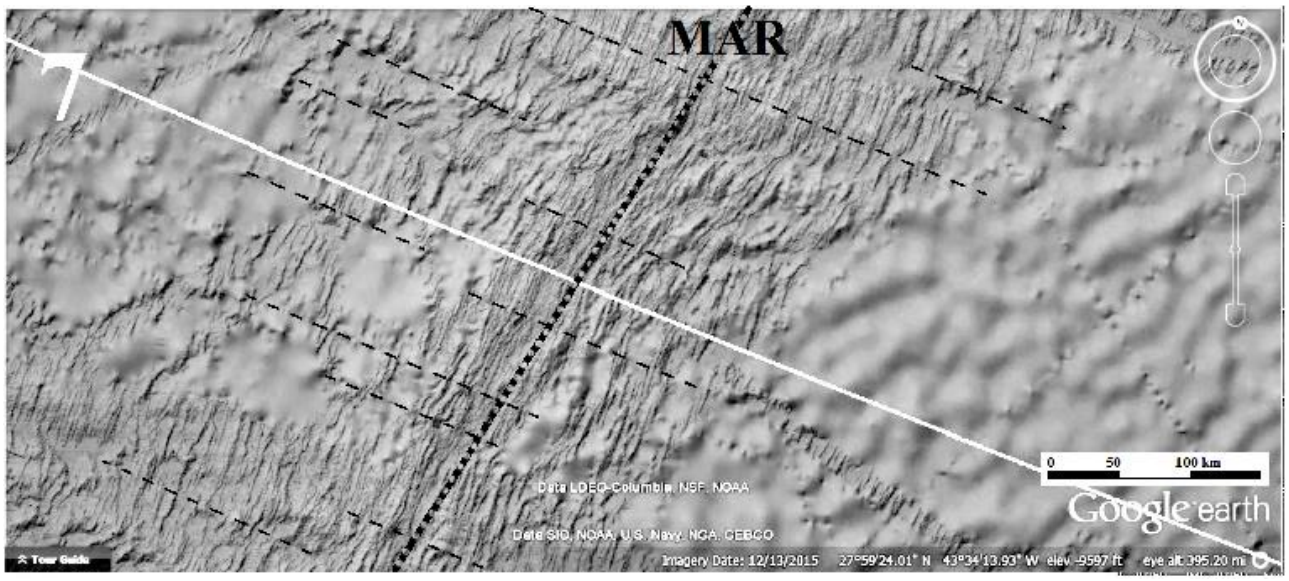

Figure 4.8: Google Earth of CGRS 7 intersecting the MAR. Concentric linears indicated by dashed lines. Other lineaments are visible. MAR, heavy dotted line, appears as tightly repeated lineaments from another center. (Google Earth, accessed 4/29/2016.)

If CGRS are global, they should be visible on land too. Figure 4.9 shows CGRS 7 moving from the Pacific onto North America, at Los Angeles, California. Concentric, prominent linears are abundant, hidden by sediments on the Continental Shelf and in the Great Valley, but clearly seen crossing the Coastal Ranges and Sierra Nevada Mountains.

CGRS 7 is about 50 km (31 miles) south of concentric linear “a” and about 40 km (25 miles) north of “b”. These distances are consistent with the 50-75 km width in the Murry FZ (Figure 4.7). Pronounced linears separated by the same distances are seen in Figure 4.8 where Pacific CGRS 7 crosses the MAR. Occurrence of similar patterns of expression over half of the circumference of the Earth requires more than happenstance.

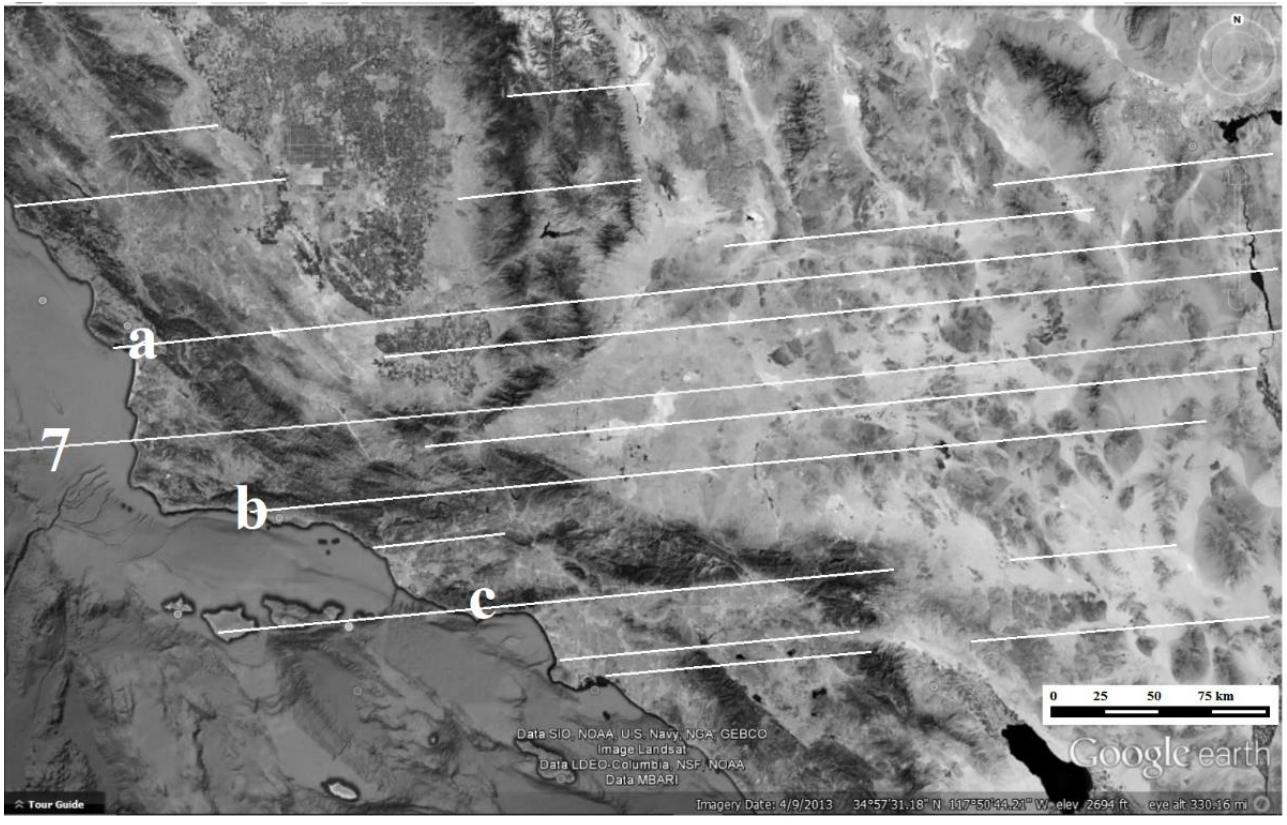

Figure 4.9: CGRS 7 moving from the Pacific basin onto land. White lines indicate concentric linears. Linear “c” can be extended across Continental shelf to the offshore islands. (Google Earth, accessed 2/11/2016.)

These multiple expressions of CGRS 7 are compared in greater detail (Figure 4.10), and seen to extend the pattern of smaller concentric linears from the prominent FZ region of the mid Pacific to the MAR. Although the CGRS cannot be traced for every kilometer of the circumference, primarily due to cultivated land and vegetative cover, this similar pattern is indication that an energy wave large enough to encircle the globe has left the same pattern expressed in the same wave or wave train.

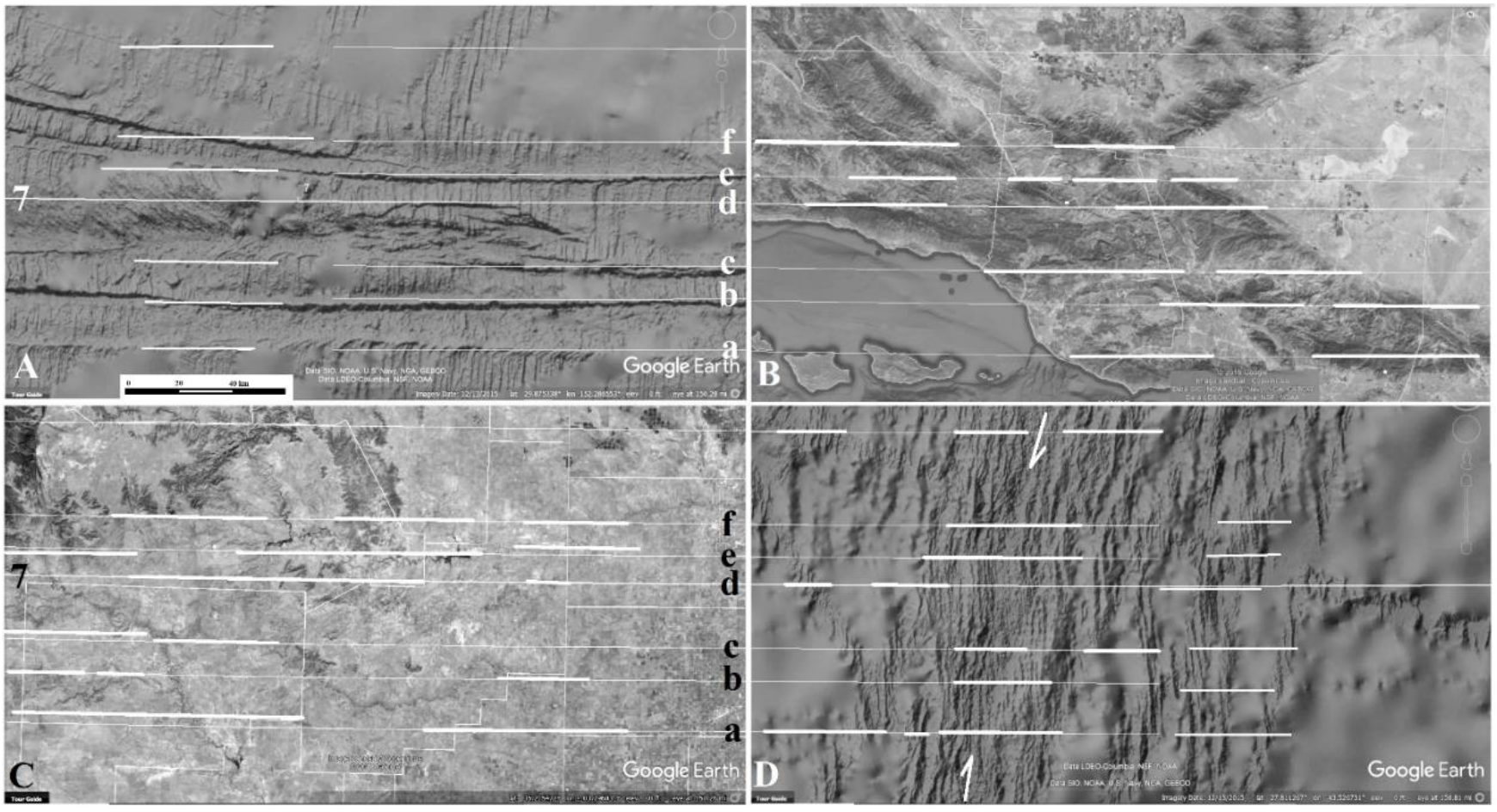

Figure 4.10: Four views of CGRS 7 and associated linears. Bolder white lines indicate regions of linear expression. (A) Murry FZ showing the natural deviation, mid Pacific. (B) Santa Barbara to Los Angeles, California. (C) Red River Valley, Texas-Oklahoma border. (D) Mid Atlantic Ridge region. White arrows indicate MAR. (Image details: Google Earth 2018, A: 29.875338°N, -152.286553°E, B: 34.554488°N, -119.430539°E, C: 35.205472°N, -103.796031°E, D: 27.811267°N, -43.526731°E. December 13, 2015, accessed 3/28/2018.)

Pacific CGRS 8, the Molokai FZ

Figure 4.11 shows CGRS 8 along the Molokai FZ. It is the most prominent in a wide region of repetitive linears where Atwater et al (1993) suggested the Pacific plate stalled or turned in its motion. It is a collection of sets of nearly parallel linears which all terminate on the southwest by a third linear. Assuming different CGRS result from different centers, the interweaving of two linears in a plastic manner from separate centers suggest their common occurrence in a common time frame. Additionally, the common termination on the southwest by a linear from another center suggest it is also a part of this same time frame.

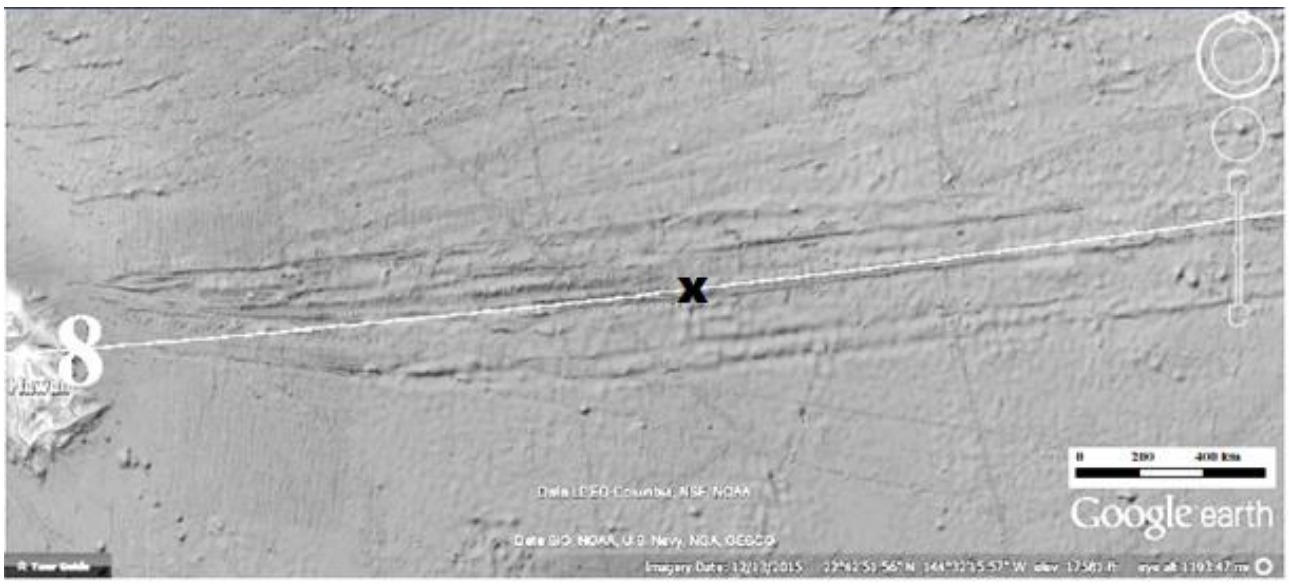

Figure 4.11: Google Earth image of CGRS 8 east of Hawaii, along the Molokai FZ. X = point on Table I. (Google Earth, accessed 4/28/2016.)

Figure 4.12 shows CGRS 8 at the Mid-Atlantic Ridge lying south of a 100-km wide trough. Note the same configuration in Figure 4.11 where a prominent trough extends 100 km to the north. Repetition of repeated landforms separated this far, reinforces genesis from a common source of point shear.

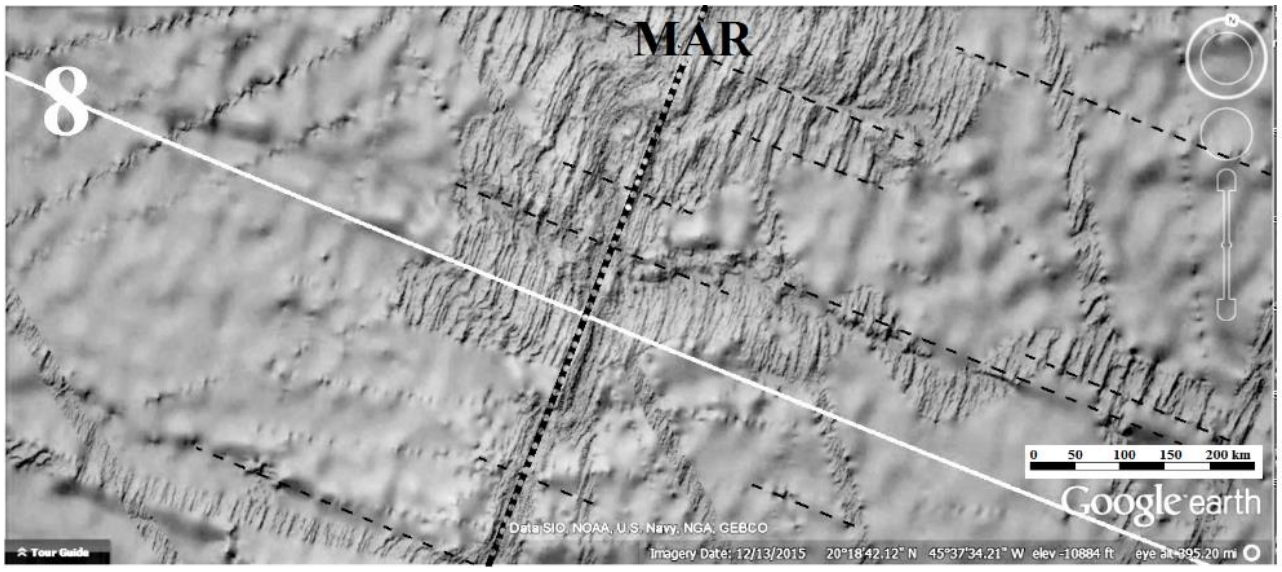

Figure 4.12: CGRS 8 at the Mid-Atlantic Ridge. Concentric linears (dashed lines) are more pronounced than the designated path of CGRS 8. (Google Earth, accessed 5/31/2016.)

In Figure 4.13, Pacific CGRS 7-9 cross New Guinea and Melanesia. Unlike Figure 4.11, which shows a broad exposure of the ring structure, this area is much more confused. However, the linears are more visible on a GGA map than on Landsat or Vertical Gravity Gradient. Lithology plays a more significant role here.

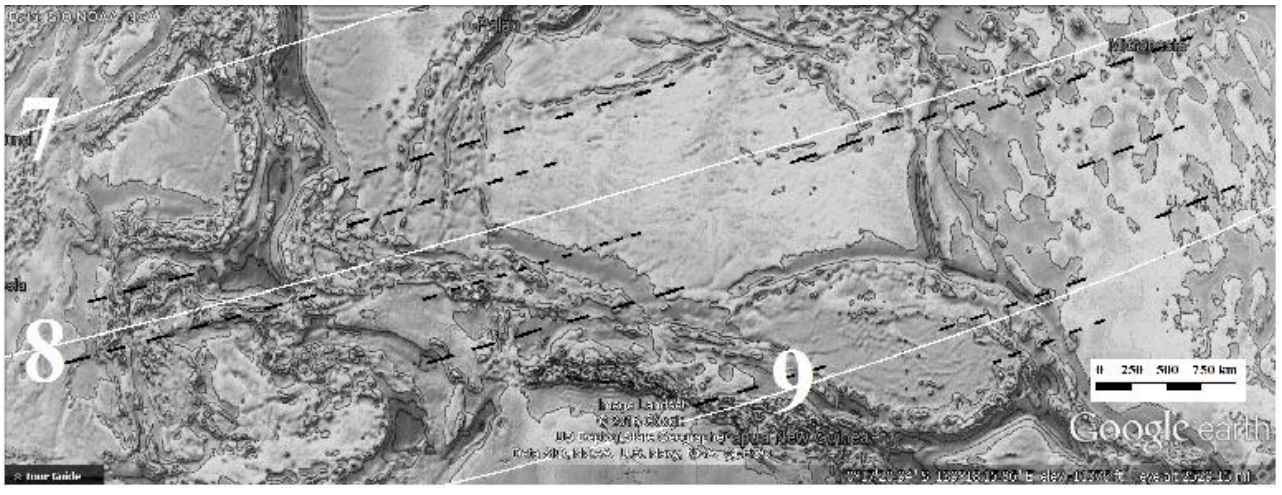

Figure 4.13: CGRS 7-9, white lines, crossing the area of New Guinea. Dashed lines indicate concentric linears. (Google Earth with Global Gravity Anomaly overlay, Scripps 2014, accessed 8/7/2016.)

More irregular expressions

Pacific CGRS 1-4

Pacific CGRS 1-4 do not include any FZ and evidence of the pressure wave is more like that seen in Unaweep and TONCK (Barnhart 2017) where we looked for points of change in the gravity patterns.

Center and antipode

CGRS 6-8 show a center at 72.7085^{o} N, 78.0330^{o} E (Table 1), Yenisei Bay, Kara Sea, Siberia, of the Arctic Ocean (Figure 4.1B and 4.14). Although few linears can be seen in the Landsat image, Figure 4.14A, as indicated by the pairs of black arrows, many more are seen in (B) Global Gravity Anomaly. Radii are a= 1000 km (620 miles), b= 820 km (509 miles), c= 520 km (323 miles) and d= 200 km (124 miles). Distinct changes in gravity reading are indicated with pairs of black arrows. These are interpreted as impact-caused ripples in the regolith and rising basalt causing bands of denser materials. Circle (A) may be the linear associated with the crater rim. Figure 4.14B shows the linear on the left of Figure 1B in Vertical Gravity Gradient is a valley corresponding to the expression of the release wave, and comparing it to the Unaweep Valley (Barnhart 2017) would suggest (a) is possibly the original crater rim.

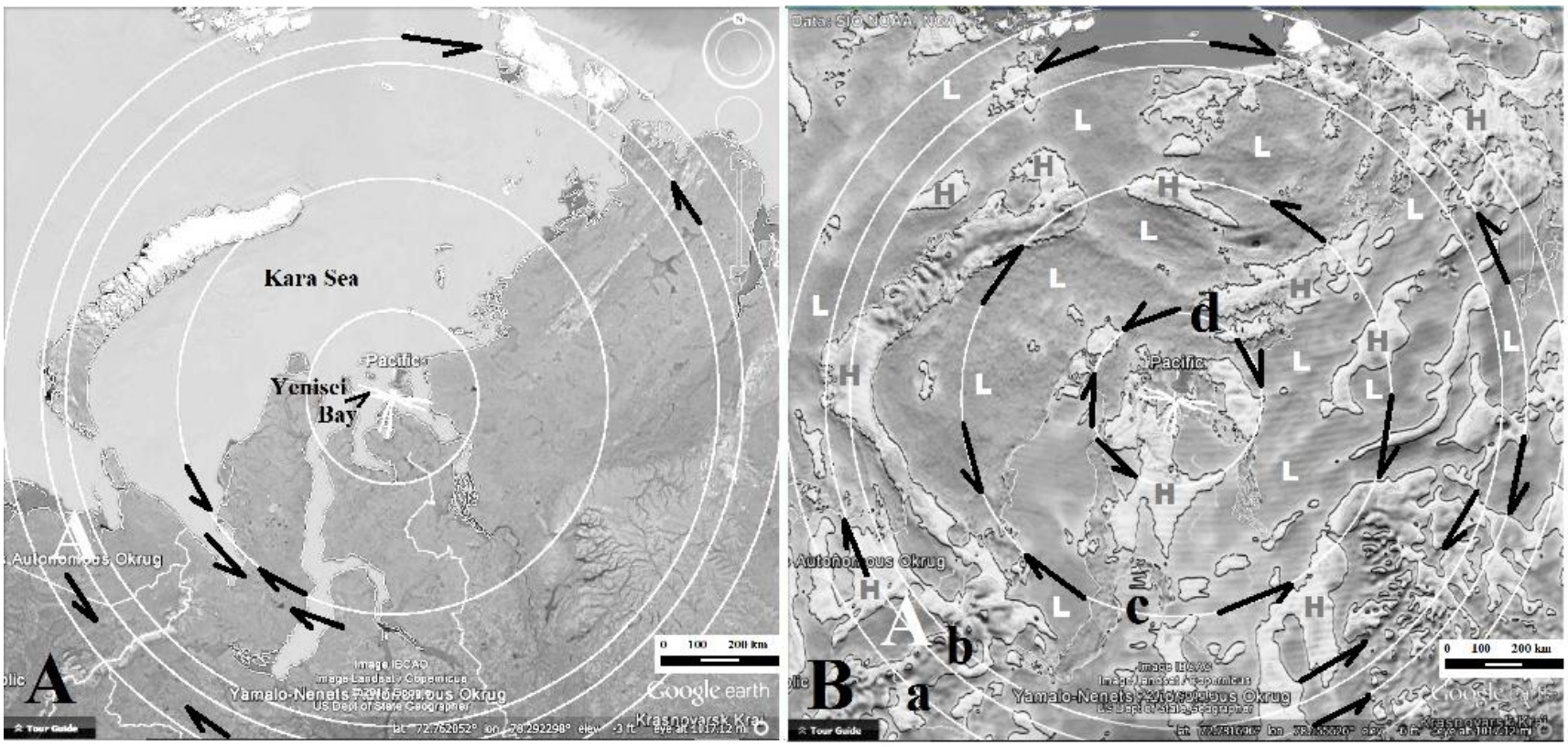

Figure 4.14: (A) Google Earth image and (B) GGA image of center for CGRS A. Linears are indicated by pairs of arrows. (A: Google Earth B: Overlay, Scripps 2014, accessed 11/1/2017.)

Pacific CGRS A and 1

CGRS 1 maps as a triple ring (Figure 4.15). Each is a distinctive linear, but (a) and (c) are distinct lines of elevated gravity while (b) is a pronounced gravity low. This triple lineament is interpreted as two shock waves with a release wave between them. This arrangement is also seen in ring A and both occurrences show the center is a complex crater with multiple rings of ridges formed by slumping blocks of crust (USRA 2016). One of these CGRS would thus represent three distinct rings of an original crater rim (Figure 4.15). At present it would be impossible to determine which, but CGRS A would give a crater width of about 2000 km (1240 miles) diameter and CGRS 1 would give a crater width of about 3000 km (1860 miles) diameter. The South Pole-Aiken Basin, the largest crater on the Moon, is 2,400 km (1,500 miles) diameter (NASA 2010) but may represent a similar expenditure of energy as CGRS 1, based on the difference in gravitational attraction of the Moon and Earth.

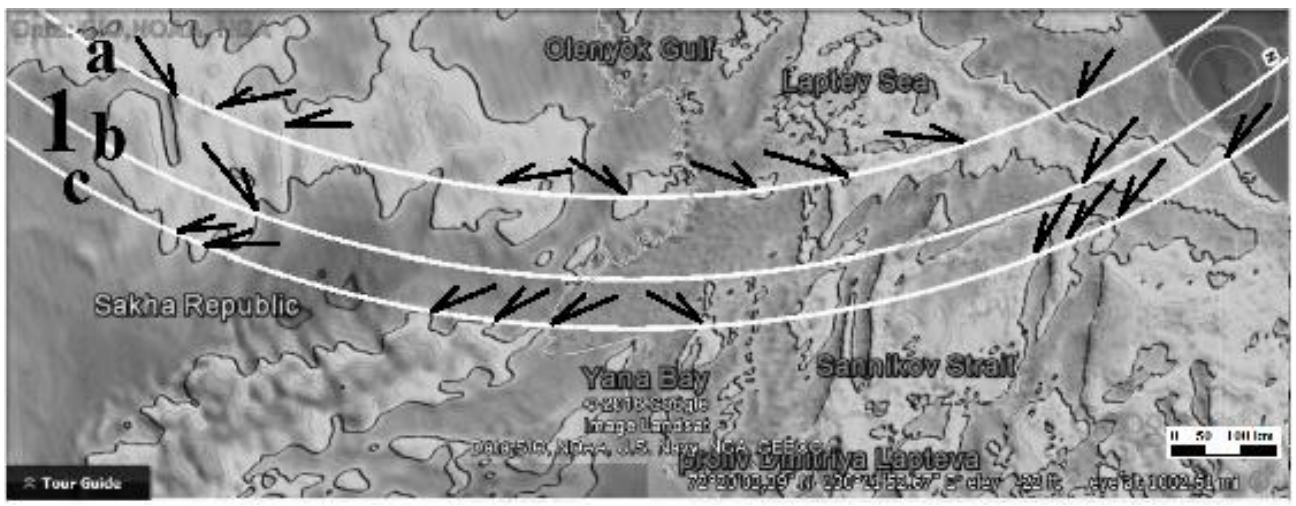

Figure 4.15: Three lines of CGRS associated with ring 1. Arrows show points of change that identify the lines. (Google Earth, accessed 5/6/2016.)

CGRS 1a and c would then be the ridges of slump blocks that moved inwards from the original crater rim, separated by the release valley (Figure 4.16A). Pacific CGRS may have been a fault. Or, it may represent an actual rift between a and c infilled with rubble (Figure 4.16B) or it may be only a depression from the release wave as in Unaweep Valley (Barnhart 2017).

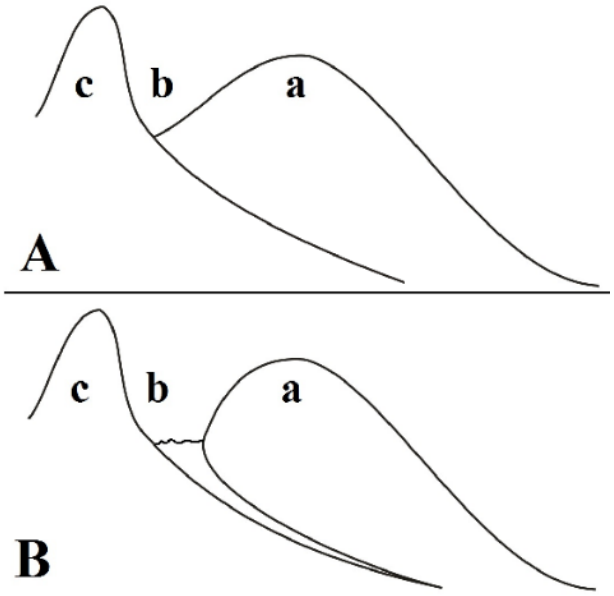

Figure 4.16: The three lines of CGRS 1 in cross section, with (a) representing the peak of the slump block sliding away from the (c) transient rim towards the center of the crater. Line (b) may have occurred in one of two ways; either (A) forming a release valley or (B) where an actual rift occurs in the rock as a result of the release wave and the adiabatic event. The rift valley is filled with rubble derived from peaks “a” and “b” and fallback rubble/ ejecta expelled from the crater.

Pacific CGRS 2-4

CGRS 2 is seen on the GGA image, Figure 4.17, as two equally-distinct expressions at the average wave length of Pacific CGRS from 1 mapped using gravity highs. Both ring sections give less distinct indication of a following gravity low.

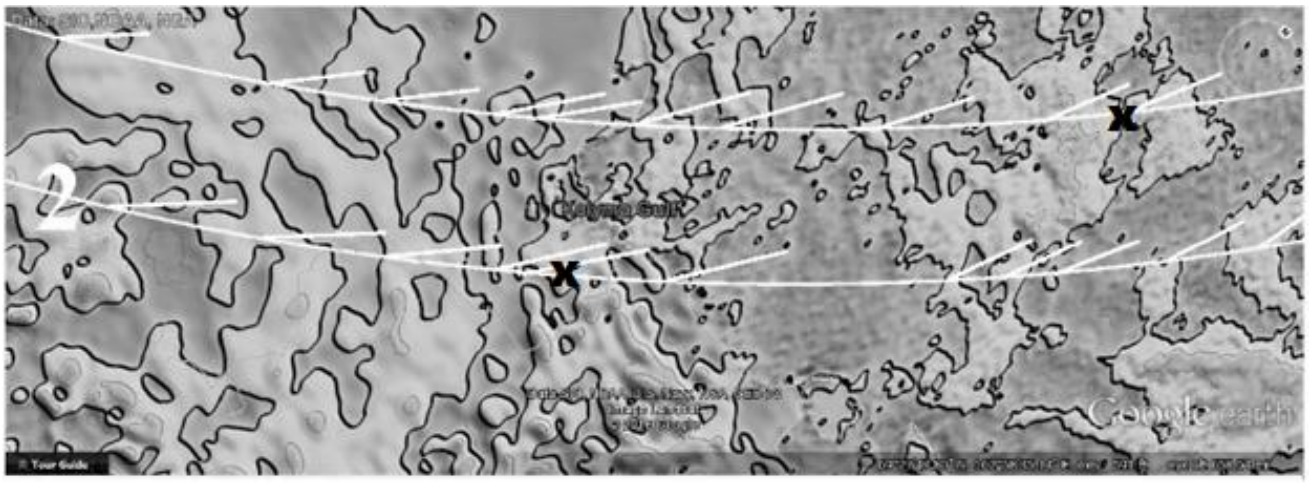

Figure 4.17: Global Gravity Anomaly image of CGRS 2 showing points of elevated gravity readings consistent with the occurrence of a ring section at both of these lines. X = point on Table I. (Google Earth, accessed 4/28/2016.)

Figure 4.18 shows CGRS 3 on a gravity high in the center of a low gravity trough. Careful observation of the peaks shows their connection with circular linears crossing the ring section. Black arrows point to lines of elevated gravity readings in front and behind the trough that would be consistent with the line corresponding to a release valley.

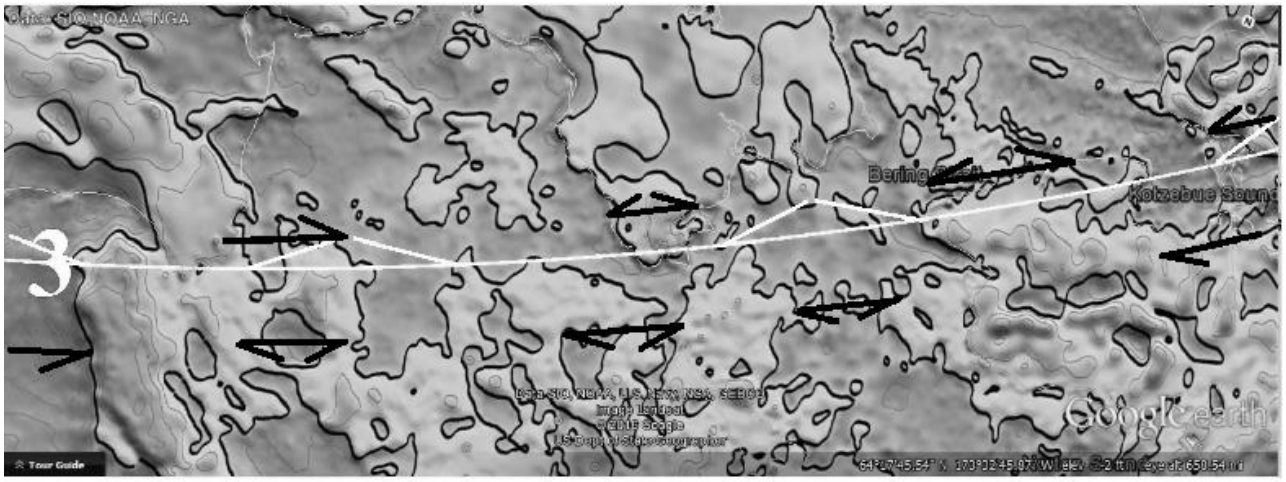

Figure 4.18: Global Gravity Anomaly overlay of CGRS 3 showing gravity readings that suggest a CGRS. Sections between opposing arrows indicate a circular lineament. Much of CGRS 3 lies in a gravity low, which could be a release valley. The black arrows indicate gravity highs corresponding with the shock and rebound waves. (Google Earth, accessed 4/28/2016.)

Figure 4.19 is a Global Gravity Anomaly image of CGRS 4 as it crosses the arc of the Aleutian Islands. GGA images do not solely show differences in topography, although it is broadly assumed color changes in GGA are associated with topographical changes (Sandwell et al 2014). Topography and GGA readings may show significant correspondence, but a casual comparison with a known surface, such as the locations in Figures 4.23 and 4.24 will show many specific areas of non-correspondence possibly reflecting lithologic differences. Lineaments for the CGRS are not always the most prominent because they are overprinted. Ridges, marked with black arrows, Figure 4.19, were from another center, and overprinted CGRS 4.

Figure 4.19: Global Gravity Anomaly overlay of CGRS 4 showing two major directions of CGRS causing a complex signature. Five or more obvious arcuate lineaments cross CGRS 4, running NE/SW (black arrows). The shift from elevated to lowered gravity readings suggests interference. Clear changes expressed in both highs and lows can be seen in the linears. X = point on Table I. (Google Earth, accessed 8/20/2016.)

Eastern China, South Korea and Japan are shown in the most significant expression of a Pacific CGRS on land. Figure 4.20 compares the Landsat view of (B) to the GGA view of (A), and it can be seen that CGRS 4 determines the south end of the Korean peninsula and the linear arrangement underpinning the circular arcs of the Islands of Japan, as well as sea ridges.

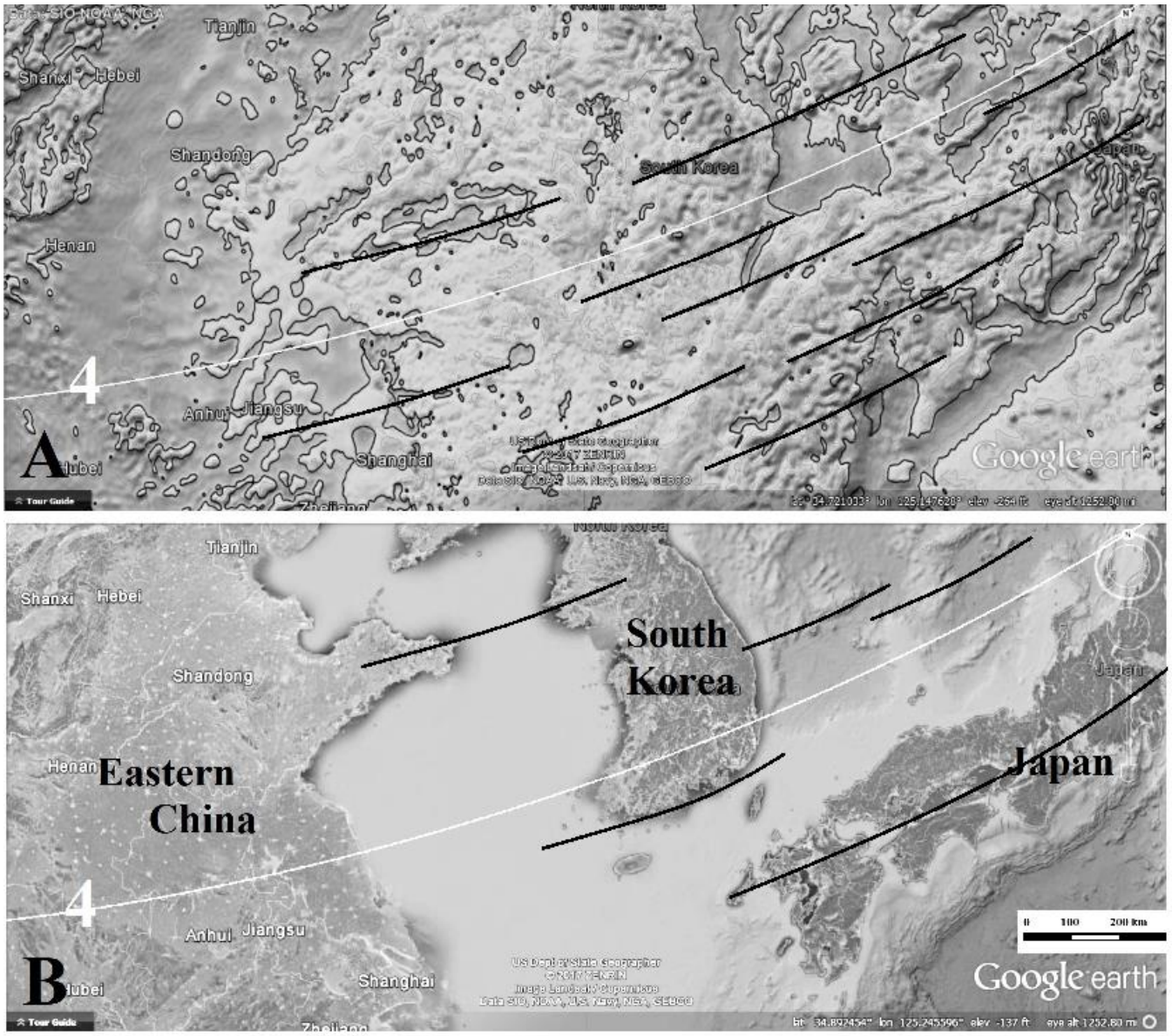

Figure 4.20: (A) Global Gravity Anomaly image of CGRS 4 crossing eastern China to Japan. (B) Landsat image of the same area showing different concentric linears. (Google Earth with overlay, Scripps 2014, accessed 11/1/2017.)

Pacific CGRS 9-18

Figure 4.21 shows CGRS 9-12 with their interruption by the Line Island Ridge, another CGRS center's expression. The multiplicity of concentric linears, black arrows, demonstrate the consistency of expression from the same center and point to their common genetic origin from Pacific center. The interrupting linear shows a different interaction than in Figure 4.9, where no distance separated the linears. This distance, most visible in Figure 4.21B, suggest it was not a plastic interaction but a brittle one.

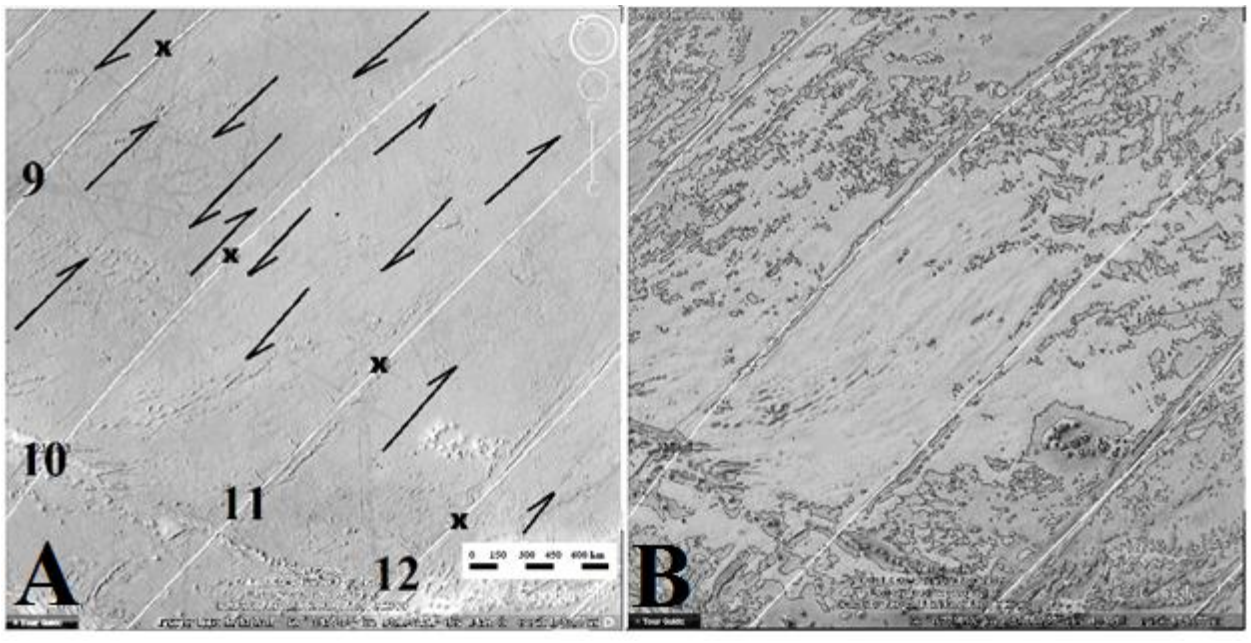

Figure 4.21: (A) CGRS 9: Clarion FZ, CGRS 10: Clipperton FZ, CGRS 11: Galapagos FZ, and CGRS 12: Marquesas FZ, with X marking points for Table 1. Arrows point to additional concentric linears. (B) Global Gravity Anomaly overlay, showing the Line Island Ridge, running diagonal across the lower third, interrupts but not touching all linears. (Google Earth with Global Gravity Anomaly, Scripps 2014, accessed 8/4/2016.)

CGRS 13 is associated with the Austral FZ, and while not as visually prominent as the more northern fracture zones, it can be traced much the same as CGRS 6-12. Finding linears south of CGRS 13, without the distinct expression of large FZ, and recognizing the almost continuous expression of ring structure through wave-trains, points are chosen for CGRS 14-18 at about 980 to 1000 km intervals, consistent with the average of CGRS 6-13. Unique gravity high points were noted in Figure 4.21 with pairs of arrows, which bridged the gap between other linears, or were unique highs crossing other linears. In some places, associated lows follow the same paths. When a concentric ring is added at that location with the already established common center, a pattern of highs and following low points occur on the line interpreted consistently with linears of the shock-release wave.

Figure 4.22: Global Gravity Anomaly overlay of the southern Pacific to Antarctica showing CGRS 13-18 and the antipode, with X marking points on Table I. (Google Earth with overlay, Scripps 2014, accessed 22/30/2017.)

Details of structure

Using shipboard data for bathymetry and the free-air gravity anomaly acquired through the Geophysical Data Center, Bonneville and McNutt (1992) provide a comparison of them at the two sections. While they do not provide specific coordinates for their sections (Figure 4.22), but do provide a small sketch of the general area, and the best correlation with the topography of the Google Earth image was made with their sketch. When the two figure for the Clarion FZ (CGRS 9) are compared it shows it as a simple shock-release wave expression (Figure 1.3, and Barnhart 2017), with a single high and low and no major interference.

Bathymetry reading reflect the bottom topography and gravity readings are thought to reflect elevation, upper crust lithology, and crustal thickness changes. Over a distance of 400 km (250 miles), variation in crustal thickness is considered negligible, so the differences between the two lines are attributed to differences in lithology. The differences between them are most pronounced before the high and after the low. The density change proceeds the high topography, and follows the low. This requires a change in lithology at the transition point. This energy expression is in keeping with the shock-release wave expression and suggest the lithologic changes led up to the topographic change and persisted as well, but changed in the exact same location. This correlation between gravity, topographic, and lithologic changes appears consistent with the expression of a CGRS composed of a shock-release wave.

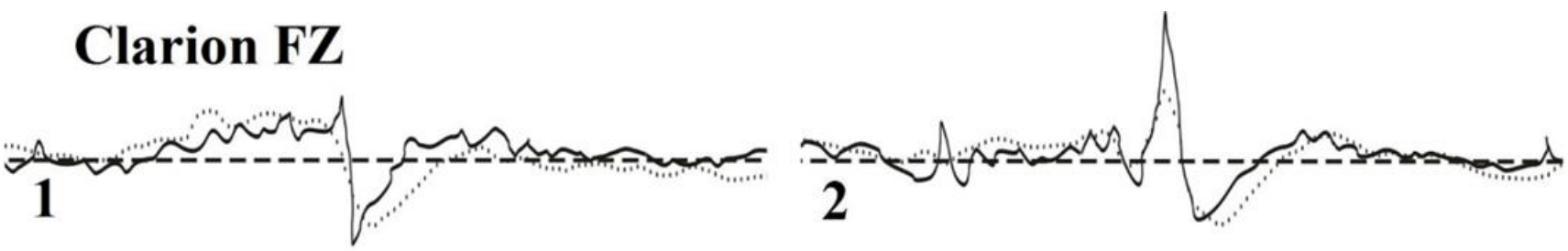

Figure 4.23: S-N cross-sections of Clarion FZ extending about 200 km in each direction from the center of the ridge slope. Solid line is topography derived from Bathymetry. Dotted line is free-air gravity anomaly. Dashed line is an arbitrary median to highlight deviation. (Image credit: modified from Bonneville and McNutt 1992.)

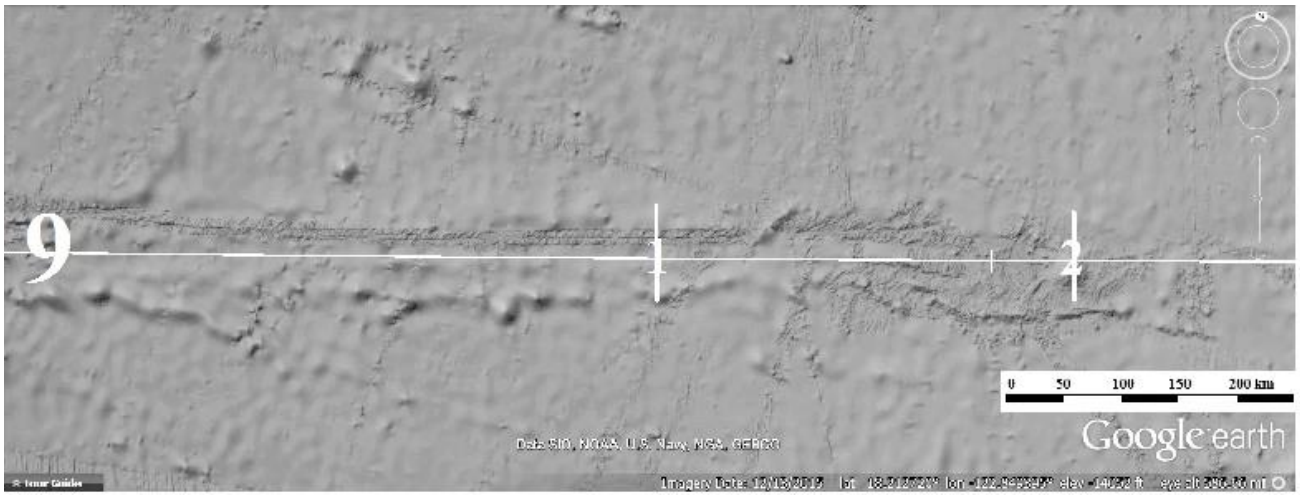

Figure 4.24: Google Earth image of Clarion FZ showing approximate locations of cross-sections in Figure 23. (2015. 18.212720°N, -122.849395°E, 13 December 2015, accessed 8/16/2016.)

Conclusion

Meyerhoff and Meyerhoff (1972) were unable to trace the west ends of Pacific FZ farther than a line extending from the Emperor Seamount Chain to the Tonga Trench and some eastern ends projecting under the continents. Additionally, Smoot and Leybourne (2001); and Smoot and Choi (2003) proposed two megatrends that they proposed crossing the entire Pacific basin and both extending into South America. That the western end extends beyond Meyerhoff and Meyerhoff's line to the west is shown in Figures 13, 20 and 22, and to the Atlantic in Figures 5, 6, 8, 10, and 12.

The highly visible sections of Pacific FZ 6-13, and indicated in Figure 4.1A, is the exception for CRGS expression, and the obscuring and plastic termination, Figure 4.10, and brittle termination, Figure 4.20, patterns through interference from other impacts is more common, leaving wave trains of smaller linear expressions.

Linking Pacific FZ to "transform" faults in the Atlantic by wave trains of concentric global linears, and continental edges and ridges in Asia show the lineaments to be global, justifying the name Concentric Global Ring Structures, and a center in Yenisei Bay, Kara Sea, Siberia.

While fracture zones are a highly visible expression of CGRS in the Pacific, other locations are less so because they have been overlaid by interference patterns from subsequent impact waves. These interactions make the form less distinct, but often leave a smaller wave train pattern.

The fault zone cross sections (Figure 4.23) show topographic and gravity profile consistent with the expression of an impact's shock-release wave following the model in Barnhart (2017), agreeing with Meyerhoff and Meyerhoff (1972, page 337), "linear magnetic anomalies of ocean basins" are not a "'taped record' of sea-floor spreading."

Acknowledgements

Deepest thanks to Maarten 't Hart, who wrote the overlay program for Google Earth to plot the CGRS and mathematically calculate their centers. Without his helpful tool, this understanding of what these lineaments represent would never have happened. "Always give yourselves fully to the work of the Lord, because you know that your labor in the Lord is not in vain" (1 Corinthians 15:58).

References

Atwater, T. 1970. Implications of Plate Tectonics for the Cenozoic tectonic evolution of western North America. *Geological Society of America Bulletin*. 81:3513-3536.

Atwater, T., J. Sclater, D. Sandwell, J. Severinghaus, M.S. Marlow 1993. Fracture Zone traces across the North Pacific Cretaceous Quiet Zone and their tectonic implications. In *The Mesozoic Pacific: Geology, Tectonics, and Volcanism.* M. S. Pringle, W. W. Sager, W. V. Sliter, and S. Stein, (editors), American Geophysical Union, Washington, D. C. pp 137-154.

Austermann, J, Z. Ben-Avraham, P. Bird, O. Heidbach, G. Schubert, and J.M. Stock. 2011. Quantifying the forces needed for the rapid change of Pacific plate motion at 6 Ma. *Earth and Planetary Science Letters* 307:289-287.

Barnhart, W.R. 2017. Cratering and the Earth: Finding a cause in Earth's lineaments, *Creation Research Society Quarterly* 53(1):191-205.

Beyer, L.A. 1971. *The vertical gradient of gravity in vertical and near-vertical boreholes*. A doctoral dissertation, Stanford University. 228 pages. sul-derivatives.stanford.edu/derivative?CSNID=00017405.../pdf, accessed 8/6/2016.

Bonneville, A. and M. McNutt. 1992. Shear strength of the great Pacific fracture zones. *Geophysical Research Letters*. 19(20): 2023-2026,

Gay, S.P. 2012.Joints, Linears, and Lineaments – The basement connection. *Search and Discovery Article #41083.* http://www.searchanddiscovery.com/pdfz/documents/2012/41083gay/ndx_gay.pdf.html, accessed 5/13/2016.

Meyerhoff, A.A. and H.A. Meyerhoff, 1972. "The new global tectonics": Age of linear magnetic anomalies of ocean basins. *AAPG Bulletin* 56(2):337-359.

Minzhang, H., L. Jiancheng, L. Hui, and X. Lelin, 2014. Bathymetry predicted from vertical gravity gradient anomalies and ship soundings. *Geodesy and Geodynamics* 5(1): 41-46,

NASA. 2010. Biggest, deepest crater exposes hidden, ancient moon. Goddard Space Flight Center. http://www.nasa.gov/centers/goddard/news/features/2010/biggest_crater.html, accessed 5/6/2016.

Sandwell, D.T. and W.H.F. Smith. 2009. Global marine gravity from retracked Geosat and ERS-1 altimetry: Ridge segmentation versus spreading rate. *Journal of Geophysical Research*. 114 (BO1411):1-18.

Sandwell, D.T., R.D. Miller, W.H.F. Smith, E. Garcia, and R. Francis. 2014. New global marine gravity CryoSat-2 and Jason-1 reveals buried tectonic structure. *Science* 346 (6205):65-67.

Scripps Institute of Oceanography. 2014. Global [Marine] Gravity Anomaly download. http://topex.ucsd.edu/grav_outreach/, accessed 11/19/2014.

Smoot, N.C. 1999, Orthogonal intersections of megatrends in the Western Pacific ocean basin: a case study of the Mid-pacific Mountains. *Geomorphology*. 20(1):323-356.

Smoot, N.C. and B.A. Leybourne, 2001. The central Pacific megatrend. *International Geology Review*. 43(4):341-365.

Smoot, N.C. and D.R. Choi. 2003. The north Pacific megatrend. *International Geology Review*. 45(4):341-365.

USRA (Universities Space Research Association). 2016. *Impact Cratering*. Lunar and Planetary Institute. http://www.lpi.usra.edu/education/explore/shaping_the_planets/impact_cratering.shtml, accessed 5/6/2016.